Effect of crystalline defects on domain wall motion under field and current in nanowires with perpendicular magnetization

F. Garcia-Sanchez,[1] H. Szambolics,[1,2] A. P. Mihai,[3,4] L. Vila,[3,4] A. Marty,[3,4] J.-P. Attané,[3,4] J.-Ch. Toussaint,[2,5] and L. D. Buda-Prejbeanu[1]

[1]*SPINTEC, UMR-8191, CEA-INAC/CNRS/UJF-Grenoble 1/Grenoble-INP, 17 Rue des Martyrs, 38054 Grenoble Cedex 9, France*

[2]*Institut Néel, CNRS, 25 Rue des Martyrs, 38042 Grenoble, France*

[3]*CEA, Inac, SP2M, Nanostructures et Magnétisme, 38054 Grenoble, France*

[4]*Université Joseph Fourier, BP 53-38041 Grenoble, France*

[5]*Institute Polytechnique de Grenoble, 46, Avenue Félix Viallet, 38031 Grenoble, France*

(Received 16 November 2009; revised manuscript received 4 February 2010; published 7 April 2010)

In this work, we present a micromagnetic study of a magnetic domain wall dynamics influenced by magnetic fields and/or spin-polarized currents in systems characterized by perpendicular magnetization including crystalline defects. The dynamics in two different systems is studied: one showing the effect of defects in the flow regime, and the second one presenting the thermally activated depinning from a single defect. In the latter case, the thermal depinning can be analyzed within the framework of a single energy barrier process. In such situation, the current density can be assimilated to an applied field. We found that the energy barrier depends linearly on the applied field and on the injected current.

DOI: 10.1103/PhysRevB.81.134408 PACS number(s): 75.40.Gb, 75.40.Mg, 75.75.−c

I. INTRODUCTION

The perspective of new applications based on domain walls[1] has renewed the interest in the dynamics of these magnetic objects. Their control through spin polarized current, theoretically predicted by Berger,[2] seems to be the most appealing choice because it allows device miniaturization. The recent progress in understanding and mastering of the current-induced domain wall (DW) motion expose the importance of DW pinning due to defects and the thermal activation phenomenon.

First, the control of DW pinning and depinning on specifically designed artificial defects (i.e., geometrical constrictions) is a prerequisite to the use of DW motion in any memory devices. In that case, the total extrinsic pinning strength is the result of the addition of the pinning due to artificial defects and that due to natural defects.

Second, perpendicularly magnetized systems appear to be more interesting than their in-plane magnetized counterpart, since they are developing thinner DW. More importantly, they are exhibiting higher efficiencies of spin transfer and DW velocities.[3,4] Since in these materials, the magnetization reversal by an applied field is mainly controlled by DW pinning, one can expect that properties like critical currents may be linked to the strength of DW pinning on natural defects,[5,6] in a similar fashion to coercive fields. The types of DWs appearing in these materials, Bloch and Néel walls, make them especially appealing for comparison with the one-dimensional (1D) analytical models of current driven DW motion.[7,8] In these models, the effect of defects[6] and temperature[9–11] has been also incorporated.

Third, the DW behavior at finite temperature is affected by thermal activation, hence motion is observed even for excitations below the zero temperature critical current and field values.[5] The thermally activated depinning is, therefore, the dominating effect on the velocity. As a result of its stochastic nature, the DW behavior is random.[12] Such effects have to be studied carefully for current-induced DW motion, especially since stochasticity was evidenced in recent DW depinning experiments.[1,13] Thus, the role of thermal activation in DW depinning cannot be neglected.

The goal of the present work is to shed a light on the randomness of the wall behavior. This study focuses on systems characterized by strong magnetocrystalline perpendicular anisotropy: CoPt multilayers and FePt $L1_0$ layers. In both systems, the DW dynamics is dominated by the natural crystalline defects occurring randomly along the sample.

By using micromagnetic modeling, we studied the viscous motion and the thermally activated depinning of a DW, using an external excitation in the form of either a magnetic field or a spin-polarized current. Both the spin transfer related effects and the thermal fluctuations were implemented in the micromagnetic solver WALL_ST.[14] In general, the combined effect of the charge current and the spin current on a DW can be split in two terms, added to the classical Landau-Lifshitz-Gilbert equation, and the final equation yielding:

$$\frac{\partial \mathbf{M}}{\partial t} = -\gamma_0 \mathbf{M} \times \mathbf{H}_{\mathbf{eff}} + \frac{\alpha}{M_s}\left(\mathbf{M} \times \frac{\partial \mathbf{M}}{\partial t}\right) - (\mathbf{u}\cdot\nabla)\mathbf{M} + \frac{\beta}{M_S}\mathbf{M} \times [(\mathbf{u}\cdot\nabla)\mathbf{M}], \quad (1)$$

where $\mathbf{u}$ is a vector pointing in the current direction with an absolute value given by $u = J_{\mathrm{app}} P g \mu_B / 2|e|M_s$ (with the dimension of a velocity). The first added term is known as the adiabatic term and the second as the nonadiabatic spin torque term. The origin of the nonadiabatic spin torque term, together with the value of the nonadiabatic spin transfer parameter, β, is still under discussion. Different physical effects have been proposed, such as spin transfer,[7,15–18] and momentum transfer.[6,19] The β value in narrow DWs is expected to be large, due to their large gradients[6] and to the small dimensions that become comparable to, or smaller than

the Fermi length[19] or the Larmor precession length.[18] The value of β is difficult to measure, and it depends on the model used to interpret the experimental data. Nevertheless, two scenarios seem to be the most plausible in both perpendicularly and longitudinally magnetized systems: $\beta \approx \alpha$ (Ref. 13) or β much larger than α.[20] Across this paper, the value of β is varied depending on the material considered. The following section, concerning CoPt nanowires, aims to explore a rather general case. β was set to 0.02, a value slightly larger than α. In the third section, a FePt system is studied with a β value varying from 0 to 1. For all simulations reported here the polarization P is chosen to be equal to 1.

The paper is organized as follows. In Sec. II, we study the influence of a random distribution of magnetocrystalline anisotropy values on the displacement of a DW. In Sec. III, we present the simulations of the thermally activated depinning from a single crystalline defect, calculating the dependence on the field and the current of the energy barrier. Finally, the conclusions are given in the Sec. IV.

II. DOMAIN WALL MOTION AND RANDOM ANISOTOPY

Most of the present theories and numerical results concerning DW motion deal with ideal systems, which might be far from real samples. For instance, it was shown that in Permalloy nanowires the characteristic defects—the surface roughness-prevented formation of antivortices.[21] This resulted in a faster motion of the walls, compared to ideal nanowires. We are interested in checking if the same behavior is observed when introducing a random anisotropy distribution in a CoPt nanowire, with out-of-plane magnetization orientation. Apparently, in such materials, crystalline defects act as very important pinning sites due to the narrowness of the wall.[22] In order to address the effect of crystalline defects on the motion of a Bloch wall, we studied their direct influence on the wall structure, and on the average wall velocity taking into account the possibility of pinning.

Following this idea, we considered a wire of size $512 \times 120 \times 11$ nm^3, divided in regular cells of $4 \times 4 \times 11$ nm^3. We used the following material parameters: the exchange stiffness $A_{ex}=1 \cdot 10^{-11}$ J/m, the saturation magnetization $M_S=254 \cdot 10^3$ A/m, the damping constant $\alpha=0.01$ (Ref. 23) and the nonadiabatic parameter $\beta=0.02$. For the ideal wire, the magnetocrystalline anisotropy (MC) constant is $K_{u,\text{ideal}}=1.27 \cdot 10^5$ J/m^3. The direction of the MC anisotropy field was kept constant along the z direction, perpendicular to the wire plane [Fig. 1(a)]. At the same time, the value of the magnetocrystalline anisotropy constant K_u was varied in each discretization cell. Two types of distributions of K_u, were generated. In the first (second) sample D1 (D2), K_u was varied in the range $[0.5,\ 1] \cdot K_{u,\text{ideal}}$ ($[0.5,\ 1.5] \cdot K_{u,\text{ideal}}$), respectively. With an average anisotropy of $\sim$75% of the $K_{u,\text{ideal}}$, sample D1 corresponds to a softer material than the initial one. In the second configuration (sample D2), the average anisotropy value is very close to the $K_{u,\text{ideal}}$. It has been determined experimentally that the length scale of the modulation of K_u is determined by the grain size, measured to be around 5–10 nm in polycrystalline films.[23] Therefore, associating anisotropy cells with the discretization cells seems to be an appropriate choice. The K_u distribution for the sample D1 is depicted in Fig. 1(a).

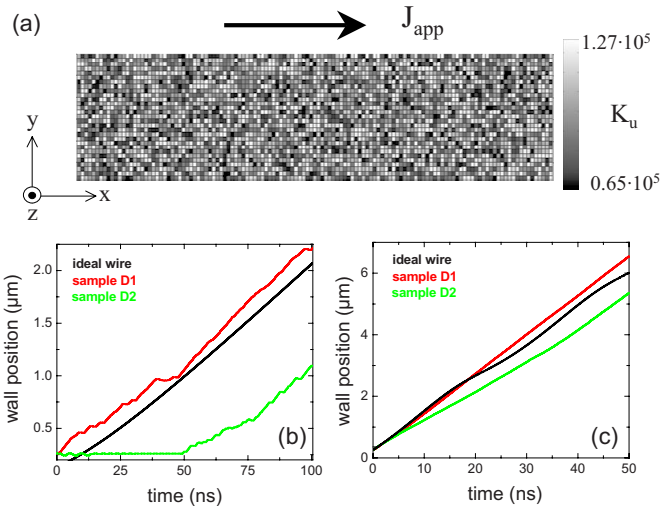

FIG. 1. (Color online) (a) Magnetocrystalline anisotropy pattern of sample D1. Time evolution of the DW position for (b) $J_{\text{app}}=5 \cdot 10^{10}$ A/m^2 and (c) $J_{\text{app}}=50 \cdot 10^{10}$ A/m^2.

We compare results obtained for an ideal (uniform K_u) CoPt-like nanowire to those obtained for wires with a random variation of K_u. In Figs. 1(b) and 1(c), the dependence of the domain wall position as a function of time is shown, for $J_{\text{app}}=5 \cdot 10^{10}$ A/m^2 and $J_{\text{app}}=50 \cdot 10^{10}$ A/m^2, respectively. Two kinds of behavior are identified:

(i) For low-current density [Fig. 1(b)], the domain wall displacement seems to be sensitive to the presence of the random anisotropy distribution, exhibiting several plateaus (red and green curves online). Furthermore, if the pinning potential is strong enough, the current values are too weak to release the DW, which stays pinned in a certain location for several tens of nanoseconds (green curve online). At this point, it is worth to note that the same kind of stochastic behavior for small values of the field is suggested by recent experimental results[12,22] of field-induced depinning.

(ii) In the high-current regime [Fig. 1(c)], the curves look similar to the ideal one, which correspond to the flow regime. As the current is increased, the curves are getting smoother suggesting that the domain wall motion is less affected by the pinning. This behavior is reminiscent to that obtained for field-induced dynamics, where current-induced DW motion undergoes a transition between a thermally activated depinning regime and a flow regime, where the dynamics is mainly governed by precession.

In Fig. 2, we show the time evolution of the wall position for current range between $5 \cdot 10^{10}$ A/m^2 and $50 \cdot 10^{10}$ A/m^2 for the sample D2. A critical current above which DW thermally assisted depinning occurs is identified around $5 \cdot 10^{10}$ A/m^2. To get rid of the natural pinning, a critical current above $20 \cdot 10^{10}$ A/m^2 must be injected. This value can be viewed as a characteristic for the transition between the low and high-current regimes.

In Fig. 3, we plot the magnetization configurations for the ideal wire and the sample D1. These configurations show

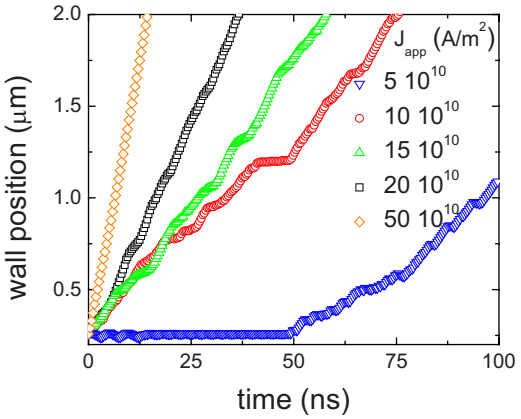

FIG. 2. (Color online) Time evolution of the domain wall position for several current values, for the sample D2.

that the DW structure in the sample D1 is far from being uniform, since very significant changes in the orientation of the magnetization occur inside the wall. Here, the DW is neither pure Bloch nor pure Néel wall type, nor the transition between these two, as in the case of the ideal wire.

It is well known that the wall velocity is intimately related to the domain wall structure. If the domain wall is of pure Bloch or pure Néel type, the wall has zero velocity. On the other hand, a transition from one configuration to the other causes the velocity to oscillate between minimal and maximal values. These observations were valid for the ideal systems, but, as we reported earlier, the magnetization orientation is not uniform inside the domain wall, in a wire with anisotropy distribution. From the displacement versus time curves in case of high-current densities, where pinning is negligible, the effective velocity has a similar value to the ideal wire. These values seem to be slightly affected by the disorder. For example, if $J_{app}=50\cdot10^{10}$ A/m^2, the velocity in the ideal wire is 113 m/s, whereas for D1(D2) sample a value of 126 m/s (103 m/s) is obtained. The same holds for the smaller current of $J_{app}=20\cdot10^{10}$ A/m^2, where the values are: for the ideal wire 51m/s, with D1 37m/s and with D2 45m/s.

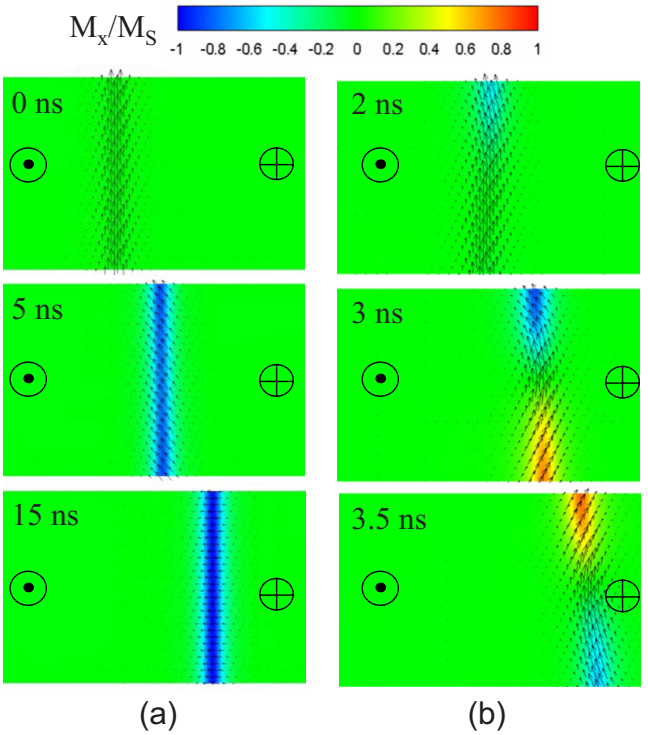

FIG. 3. (Color online) Magnetization distribution at several times, for the ideal wire (a), and for the sample D1 (b). The injected current is $J_{app}=50\cdot10^{10}$ A/m^2. The area represented is 240×120 nm^2.

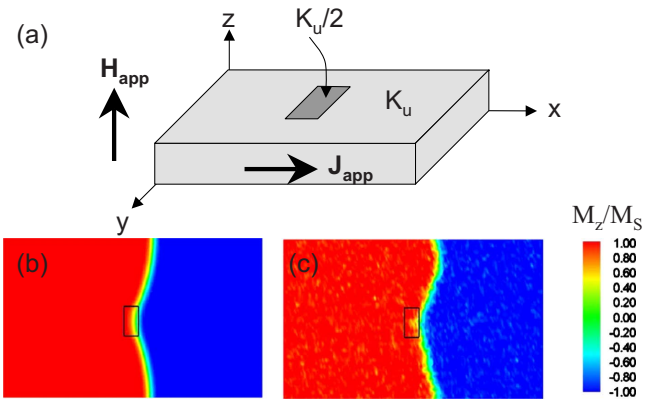

FIG. 4. (Color online) (a) Schematic view of the system and coordinates. (b) Equilibrium state under applied field $\mu_0H_{app}=0.18$ T at $T=0$ K. (c) Configuration at $T=400$ K corresponding to one depinning event.

During its displacement, the domain wall will try to avoid the regions with high anisotropy and in counterbalance to favor the regions with low anisotropy. As a consequence, the domain wall movement might be stopped, and the domain wall pinned if the energy barrier to overcome is too high.

III. THERMAL DEPINNING FROM SINGLE DEFECT

In this section, we study the effect of a single crystalline defect, to gain a deeper insight on the pinning and depinning processes. For this purpose, we simulated wires tailored in FePt/MgO thin films, with very large crystal anisotropy.[24]

The simulated sample has a size of $80\times50\times5$ nm^3 and includes a defect in the center with a size of $5\times10\times5$ nm^3 [Fig. 4(a)]. The material parameters are: $K_u=5\cdot10^6$ J/m^3, $A_{ex}=6.9\cdot10^{-12}$ J/m and $M_S=1.03\cdot10^6$ A/m. For the damping parameter, a value of $\alpha=0.1$ was used.[25] The easy axis of the material is perpendicular to sample plane (z direction). Such materials are known to form narrow domain walls (Bloch parameter $\Delta=\sqrt{A_{ex}/K_u}=1.17$ nm), so in order to ensure a good accuracy, the system has been discretized in cells of size $\Delta_x\times\Delta_y\times\Delta_z=0.5\times1\times5$ nm^3. The defect is modeled as a region with a lower anisotropy constant $K_{def}=0.5$ K_u, keeping the rest of parameters unchanged. The calculated depinning field at 0 K, for a domain wall pinned at the defect in this sample is found to be $\mu_0H_{dep}(T=0\text{ K})=0.225$ T, which is of the same order of magnitude as the coercitive field measured in these materials.

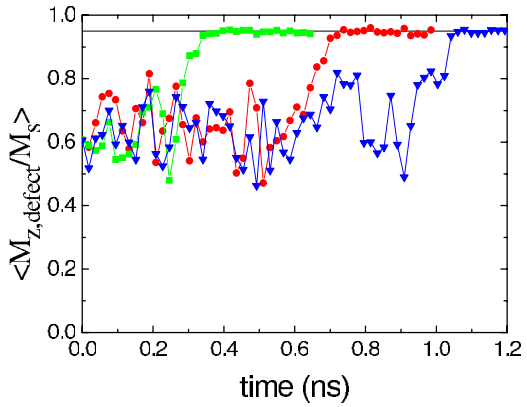

FIG. 5. (Color online) Time evolution of mean value of M_z/M_S calculated inside the defect for three different events. The applied field is $\mu_0 H_{app}$=0.18 T at T=400 K. The black line is the value $\langle M_z/M_S\rangle$=0.95, which corresponds to the depinning criterion.

A magnetic field lower than the depinning field is applied in the z direction and the sample temperature T was kept 400 K. The temperature was included in the form of a Gaussian distributed thermal field $\boldsymbol{H_{th}}$, which is added to the total effective field. The thermal fluctuations have the following properties:[26]

$$\langle H_{th,i}(t)\rangle = 0, \tag{2}$$

$$\langle H_{th,i}(t)H_{th,i}(t')\rangle = \frac{2\alpha k_B T}{\gamma_0 \mu_0 M_S \Delta_x \Delta_y \Delta_z}\delta ij\,\delta(t-t'), \tag{3}$$

where k_B is the Boltzmann constant. The initial configuration, corresponding to the zero temperature equilibrium, contains a DW pinned on the defect. The DW character is not purely Bloch type, but, due to the presence of the defect, is a two-dimensional one [Fig. 4(b)]. The magnetization in the defect region as a function of time is plotted in Fig. 5, for several depinning events. During the initial stages, the magnetization evolves under the effect of thermal fluctuations, and, after several attempts, DW successfully overcomes the barrier, and gets out of the box defined by the defect [Fig. 4(c)]. We define the depinning time as the one at which the value of $\langle M_z/M_S\rangle$ becomes larger than 0.95 (Fig. 5). After the depinning, the DW will move under the effect of the applied excitation, but this motion is not relevant for the experiments of thermal depinning. The dynamics prior to depinning is in the range of nanoseconds, while the experiments of thermal depinning can extend to the scale of seconds. However, due to the limitations in the computing time, we restricted our computations to 100 ns. We repeated the simulations several hundred times (at least 200), to ensure enough statistics, for plotting the distribution of number of events with determined depinning time. This allows the evaluation of the cumulative distribution function, which gives the probability of being depinned after time t.

The analysis of the thermally activated processes is in general a complicated task. However, if the process corresponds to the crossing of a single energy barrier and that barrier is much larger than the thermal energy,

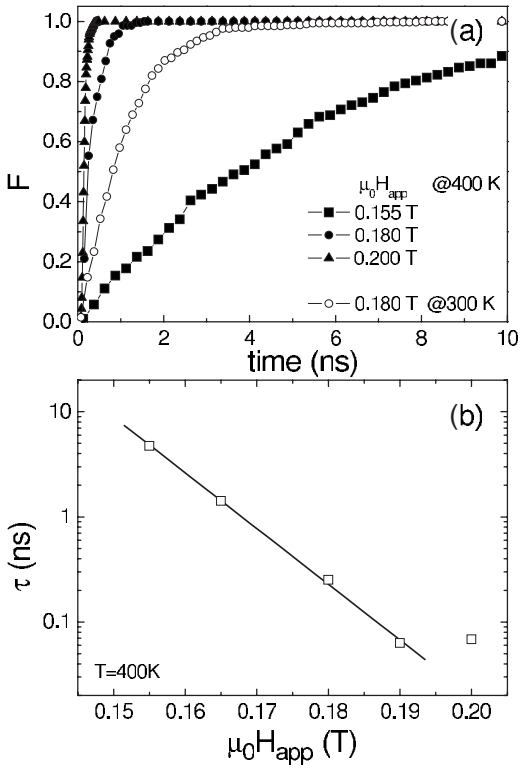

FIG. 6. (a) Cumulative probability of depinning as a function of time for different applied field values and no current. (b) Depinnig time constant variation with the applied field at T=400 K.

(i.e., $E_B \gg k_B T$, where E_B is the energy barrier that the DW has to overcome), the process can be described by an exponential probability law.[26,27] In that case, the cumulative distribution function is

$$F(t) = 1 - \exp\left(-\frac{t}{\tau}\right), \tag{4}$$

where τ is the Arrhenius-Néel relaxation time, given by $\tau = \tau_0 \exp(E_B/k_B T)$, where τ_0 is the attempt frequency.

Figure 6(a) shows the cumulative probability for different applied fields. For the smallest field value at T=400 K, the simulations confirm the exponential law, in accordance with experimental results.[12] In this case, it is clear that thermal activation is observed in our simulation with an apparent single energy barrier process. This also holds well for the curve calculated at T=300 K and $\mu_0 H_{app}$=0.18 T [Fig. 6(a), open circles]. The exponential law for the cumulative probability does not hold for larger field values, at T=400 K. This fact can be explained assuming two different time scales in the depinning, one corresponding to the time scale of thermal activation, and the other corresponding to the time in which the successful event takes place (see Fig. 5). When both time scales are comparable, the exponential law is not obeyed.

In Fig. 6(b), we plot the time parameter τ as a function of the applied field, for T=400 K. If the cumulative distribution follows Eq. (2), the average depinning time becomes equal to τ. Increasing the applied field reduces the average depinning time. The fitting of the logarithm of τ versus field

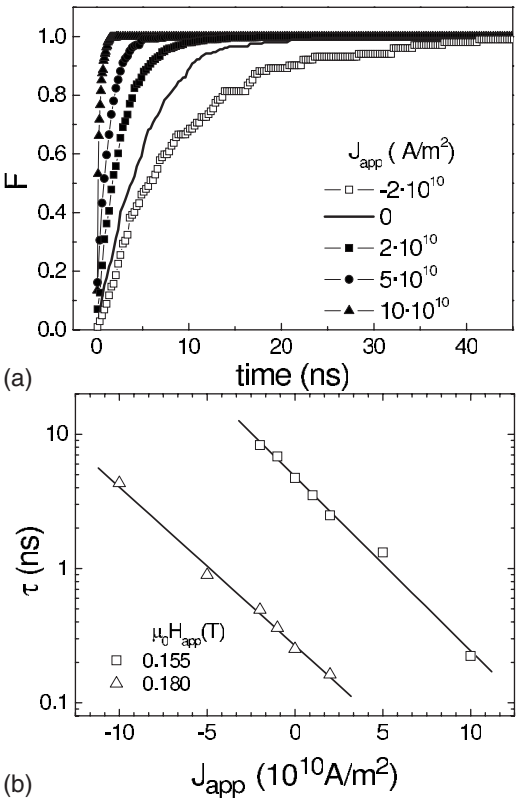

FIG. 7. (a) Cumulative probability of depinning as a function of time at $T=400$ K for $\mu_0 H_{app}=0.155$ T with $\beta=1$ and different injected current values. (b) Depinnig time constant variation with the injected current at $T=400$ K.

yields the dependence of E_B on the applied field, considering that the attempt frequency τ_0 is independent or slightly dependent on the field values. For quite a large range of applied fields, we found a linear dependence of the energy barrier on the field value. Thus, we can express the energy barrier as:

$$E_B = 2M_s V(H_{dep} - H_{app}) = a_H H_{app} + b_H, \tag{5}$$

where V is the activation volume. This expression represents the weak pinning limit,[28] and was confirmed experimentally.[12] However, there are differences in the time scales and the actual value of depinning fields. The first one can be assigned to the difficulties in extending our calculation beyond the nanosecond time scale, the latter to the lack of an accurate model for the defect. Nevertheless, the physics of the system is preserved, and the same behavior is obtained. From our simulations we deduced an activation volume of $V=327$ nm^3. We can define the length of the energy barrier dividing the activation volume by the cross section of the defect. The length is equal to 6.55 nm, which is larger than the length of the defect (5 nm). This indicates that energy barrier is comparable to the difference in the Zeeman energy corresponding to the defect magnetization reversal, but the thermal mechanism is still an inhomogeneous process.

In the following, we fixed the magnetic field and applied current densities flowing parallel to the long axis of the wire (x direction). Figure 7(a) shows the cumulative probability

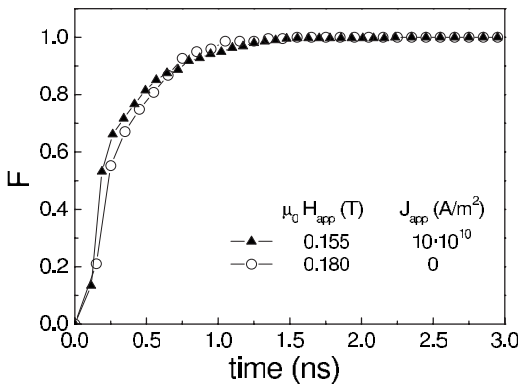

FIG. 8. Equivalence between injected the effects of current and applied field.

for different current densities, for $\mu_0 H_{app}=0.155$ T. Since the origin of the nonadiabatic term can be assigned to the mistracking of the electron spins with respect to the local magnetization direction, the nonadiabatic term is expected to have larger values in perpendicular anisotropy materials, where the domain walls are narrow and comparable to the characteristic lengths of the electrons. For this reason we choose a value of $\beta=1$ throughout this section.

An appreciable effect on the average depinning time is observed even at low-current densities. Moreover, an asymmetric behavior of the probability with respect to the current polarity is present. The effect of negative current is to slow down the depinning, while positive current reduces the depinning time. This result is also consistent with the experimental observations.[13] In Fig. 7(b), we plot the time constant versus the current density for two different applied field values. Again, we observed a linear dependence of the energy barrier on the current density

$$E_B(J_{app}) = a_J J_{app} + b_J, \tag{6}$$

which was also obtained experimentally.[13] The slope of the curves in Fig. 7(b) is slightly different for the two field values. In general a_J is field dependent because the field value will alter the gradient of the magnetization according to the Eq. (1). The linear dependence and the parameter a_J have been derived from the Fokker-Planck equation, in a 1D model of thermal activation.[10,11]

In the one dimensional model of DW motion without thermal activation, the nonadiabatic term is equivalent to an applied field.[7] This equivalence suggests an experimental procedure to measure the value of β. In the case of thermal activation, we found that the effects of currents and fields are similar, as $\ln(t)$ is proportional to both H_{app} and J_{app}. We can thus establish equivalence between two sets of current and field values, which have the same depinning probability distributions and, therefore, equal average depinning times. This is shown in Fig. 8 for two different sets of parameters. In this case, the equivalent field for the given current is the difference between the corresponding applied field values of the sets. We define the efficiency ξ as the ratio between the equivalent field and the current density as[7]

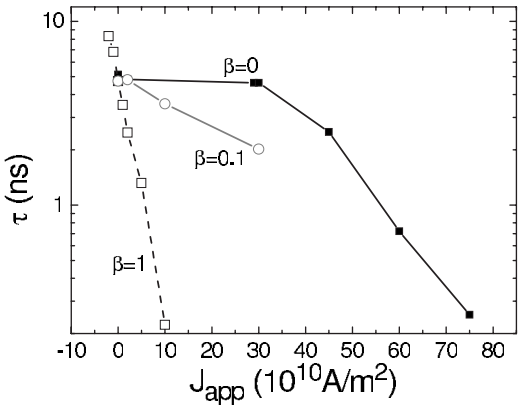

FIG. 9. Depinnig time constant variation with the injected current at $T=400$ K and $\mu_0 H_{app}=0.155$ T, for different values of the nonadiabatic parameter.

$$\xi = \frac{\beta P \hbar}{2|e|M_S \Delta}. \tag{7}$$

However, this 1D formula for the efficiency is not valid for our nanowire, since we are studying thermal activation in the framework of a three-dimensional (3D) micromagnetic model. In our simulations, we found that there is a linear relation between the energy barrier and the applied field and/or injected current. Therefore, it is easy to establish the equivalence for two sets of currents and applied fields with equal energy barrier. We calculated the efficiency as the ratio between the parameters of the energy barrier, thus obtaining a value of $\xi=a_J/a_H=2.4\cdot 10^{-13}$ Tm^2/A for $\mu_0 H_{app}=0.155$ T.

Finally, we also calculated the τ dependence on the current density in the adiabatic case, $\beta=0$, and in the case $\beta=\alpha$, and the results are shown in Fig. 9. For the case $\beta=\alpha$ and intermediate current densities, a linear dependence of the logarithm of average depinning time on current is again obtained. Equation (7) and Ref. 11 indicate a direct proportionality of the efficiency with β. In agreement with that fact, the slope in Fig. 9 for $\beta=1$ is 10 times the slope for the case $\beta=\alpha$. The adiabatic ($\beta=0$) case can be separated in two regions: one with zero slope, in agreement with the 1D formula,[11] and one with appreciable reduction for large densities, comparable to the total critical current $[J_c(T=0\ \mathrm{K})=7.75\cdot 10^{11}\ \mathrm{A/m}^2]$. In the adiabatic case, there is an additional contribution to the pinning known as intrinsic pinning[6] originated, in perpendicular anisotropy materials, by the in-plane anisotropy. The reduction of the depinning time is due to the modification of the two-dimensional (2D) equilibrium configuration produced by the applied current.

IV. CONCLUSIONS

Determination of β by dynamical measurements requires the knowledge of whether the DW motion is beyond the velocity breakdown,[7] similar to the field case Walker limit.[29] For current densities below that breakdown, the 1D model predicts a velocity proportional to β. Beyond that limit, the value of β can be obtained from the oscillation frequency of the observed structural changes, similar to those observed in Fig. 3(a). From the evolution shown in Fig. 3(b), it is clear that those oscillations will be perturbed by the presence of defects and the value of β will be not accessible. So the role played by the defect is twofold: first, it determines the critical current for the motion through extrinsic pinning, and second, it suppresses the appearance of a single frequency DW precession.

In the second case studied the model reproduces qualitatively the experiments and the analytical theory of thermal depinning due to defects. Namely, there is a linear dependence of the energy barrier on the applied field and current, and an asymmetric behavior with respect to the current. The exponential law indicates that the thermal depinnig is well described by a single barrier process. In addition, we found an equivalence between current and field, which can be expressed in the form $H_{eq}=\xi J_{app}$. However, in order to address the question about the real value of β, the proportionality factor in the linear dependence of the energy barrier has to be extracted from the theory and compared to experiment. This factor has been studied in 1D system[10,11] from a quadratic pinning potential, but an equivalent derivation is beyond the scope of this article. Finally, the results suggest that the nonadiabatic term is necessary to obtain non-negligible effect of the current for low densities. This represents an additional proof of the necessity to include a nonadiabatic term in spin transfer theories.

ACKNOWLEDGMENTS

This work has been supported by the French National Research Agency (ANR) through the ISTRADE (Project No. ANR-07-NANO-037-04) and part of numerical simulations has been carried out with the resources of IDRIS (Project No. 096048).

[1] M. Hayashi, L. Thomas, R. Moriya, C. Rettner, and S. S. P. Parkin, Science **320**, 209 (2008).
[2] L. Berger, J. Appl. Phys. **55**, 1954 (1984).
[3] S. Fukami, T. Suzuki, N. Ohshima, K. Nagahara and N. Ishiwata, J. Appl. Phys. **103**, 07E718 (2008).
[4] T. A. Moore, I. M. Miron, G. Gaudin, G. Serret, S. Auffret, B. Rodmacq, A. Schuhl, S. Pizzini, J. Vogel, and M. Bonfim, Appl. Phys. Lett. **93**, 262504 (2008).
[5] D. Ravelosona, D. Lacour, J. A. Katine, B. D. Terris and C. Chappert, Phys. Rev. Lett. **95**, 117203 (2005).
[6] G. Tatara and H. Kohno, Phys. Rev. Lett. **92**, 086601 (2004).
[7] A. Thiaville, Y. Nakatani, J. Miltat, and Y. Suzuki, Europhys. Lett. **69**, 990 (2005).
[8] A. Mougin, M. Cormier, J. P. Adam, P. J. Metaxas, and J. Ferré,

EPL **78**, 57007 (2007).
[9] R. A. Duine, A. S. Nunez, and A. H. MacDonald, Phys. Rev. Lett. **98**, 056605 (2007).
[10] M. E. Lucassen, H. J. van Driel, C. Morais Smith, and R. A. Duine, Phys. Rev. B **79**, 224411 (2009).
[11] J.-V. Kim and C. Burrowes, Phys. Rev. B **80**, 214424 (2009).
[12] J. P. Attané, D. Ravelosona, A. Marty, Y. Samson, and C. Chappert, Phys. Rev. Lett. **96**, 147204 (2006).
[13] C. Burrowes, A. P. Mihai, D. Ravelosona, J.-V. Kim, C. Chappert, L. Vila, A. Marty, Y. Samson, F. Garcia-Sanchez, L. D. Buda-Prejbeanu, I. Tudosa, E. E. Fullerton, and J.-P. Attané, Nat. Phys. **6**, 17 (2010).
[14] H. Szambolics, J. Ch. Toussaint, A. Marty, M. Miron, and L. D. Buda-Prejbeanu, J. Magn. Magn. Mater. **321**, 1912 (2009).
[15] S. Zhang and Z. Li, Phys. Rev. Lett. **93**, 127204 (2004).
[16] S. E. Barnes and S. Maekawa, Phys. Rev. Lett. **95**, 107204 (2005).
[17] Y. Tserkovnyak, H. J. Skadsem, A. Brataas, and G. E. W. Bauer, Phys. Rev. B **74**, 144405 (2006).
[18] A. Vanhaverbeke and M. Viret, Phys. Rev. B **75**, 024411 (2007).
[19] M. E. Lucassen and R. A. Duine, Phys. Rev. B **80**, 144421 (2009).
[20] O. Boulle, J. Kimling, P. Warnicke, M. Kläui, U. Rüdiger, G. Malinowski, H. J. M. Swagten, B. Koopmans, C. Ulysse, and G. Faini, Phys. Rev. Lett. **101**, 216601 (2008).
[21] Y. Nakatani, A. Thiaville, and J. Miltat, Nature Mater. **2**, 521 (2003).
[22] C. Burrowes, D. Ravelosona, C. Chappert, S. Mangin, E. E. Fullerton, J. A. Katine, and B. D. Terris, Appl. Phys. Lett. **93**, 172513 (2008).
[23] B. Rodmacq, V. Baltz, and B. Dieny, Phys. Rev. B **73**, 092405 (2006).
[24] T. Jourdan J. P. Attané, F. Lançon, C. Beigné, L. Vila, and A. Marty, J. Magn. Magn. Mater. **321**, 2187 (2009).
[25] M. Weisheit, M. Bonfim, R. Grechishkin, V. Barthem, S. Fähler, and D. Givord, IEEE Trans. Magn. **42**, 3072 (2006).
[26] W. F. Brown, Jr., Phys. Rev. **130**, 1677 (1963).
[27] L. Néel, Ann. Geophys. **5**, 99 (1949).
[28] P. Gaunt, J. Appl. Phys. **59**, 4129 (1986).
[29] N. L. Schryer and L. R. Walker, J. Appl. Phys. **45**, 5406 (1974).